

# YVO<sub>4</sub>:RE (RE = Eu, Tm, and Yb/Er) nanoparticles synthesized by the microwave-assisted hydrothermal method for photoluminescence application

Ivo Mateus Pinatti<sup>1+</sup>, Camila Cristina de Foggi<sup>2</sup>, Marcio Daldin Teodoro<sup>3</sup>, Elson Longo<sup>4</sup>, Alexandre Zirpoli Simões<sup>1</sup>, Ieda Lúcia Viana Rosa<sup>4</sup>

1. São Paulo State University, Faculty of Engineering, Guaratinguetá, Brazil.
2. Federal University of Rio Grande do Sul, School of Dentistry, Porto Alegre, Brazil.
3. Federal University of São Carlos, Department of Physics, São Carlos, Brazil.
4. Federal University of São Carlos, Center for the Development of Functional Materials, São Carlos, Brazil.

**+Corresponding author:** Ivo Mateus Pinatti, **Phone:** +55 16 33518214, **Email address:** [ivopinatti@hotmail.com](mailto:ivopinatti@hotmail.com)

## ARTICLE INFO

### Article history:

**Received:** July 29, 2021

**Accepted:** October 11, 2021

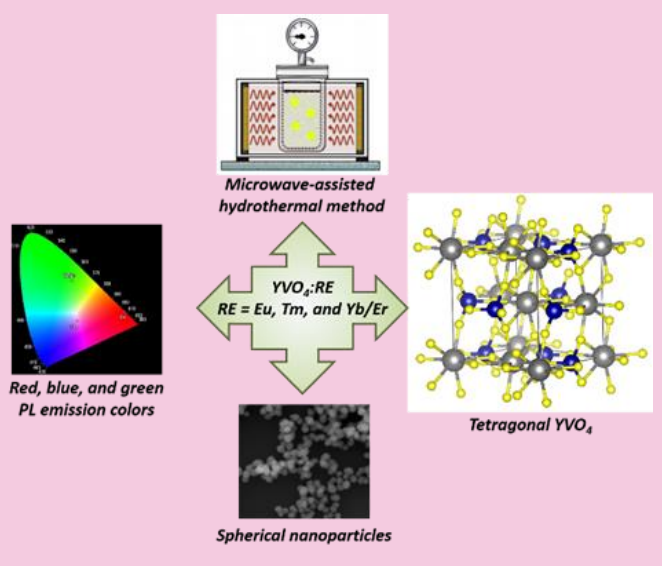
**Published:** April 11, 2022

### Keywords:

1. yttrium vanadate
2. rare earth
3. photoluminescence
4. semiconductor

*Section Editors:* Elson Longo and Juan Manuel Andrés Bort

**ABSTRACT:** Here, an experimental study is presented on the YVO<sub>4</sub>:RE (RE = Eu, Tm, and Yb/Er) nanoparticles synthesized by means of the microwave-assisted hydrothermal method. Different characterization techniques (X-ray diffraction, Raman and ultraviolet-visible spectroscopy, field emission scanning electron microscopy, transmission electron microscopy, and photoluminescence emissions) have been employed to examine the structural, optical, as well as its morphology and photoluminescent properties. The as-synthesized samples present different emission colors due to RE<sup>3+</sup> ions, as well as nanosized spherical morphology because of synthesis method. These materials can be considered efficient materials for optical devices.



## 1. Introduction

Photoluminescent (PL) materials with high quantum efficiency present practical applications in many research areas, such as optoelectronics, medicine, biolabels, physics, among others (Ferreira *et al.*, 2018; Panayiotakis *et al.*, 1996; Shen *et al.*, 2010). Consequently, several inorganic matrices are studied, in which its PL property was deeply explored due to its host lattice composition, structure, morphology as well as doping and others crystal modifications (Li *et al.*, 2021). Ideally, these materials may present well-defined characteristics such as size, optical properties, and a wide range of emission colors (Liu *et al.*, 2016).

Moreover, visible-emitting phosphors can be achieved by doping different kinds of rare earth (RE) ions into lanthanide orthovanadates. The orthovanadate matrix absorbs in the ultraviolet region of electromagnetic spectrum due to ligand-metal charge transfer (LMCT) from the 2p orbital in  $O^{2-}$  to the 3d orbital in vanadate. The  $YVO_4$  nanoparticles, as an example, are an ideal transparent host lattice for PL activators and present low toxicity in biological medium (Rivera-Enríquez and Fernández-Osorio, 2021).  $YVO_4$  also presents relative low phonon energy, excellent thermal, mechanical, and chemical stability and high optical performance. Furthermore, the  $D_{2d}$  local point symmetry of the eight-coordinated  $Y^{3+}$  ion in the tetragonal crystal structure (space group  $D_{4h}$ ) is an ideal doping site for  $RE^{3+}$  ions (Liu *et al.*, 2015). For instance, controlled fabrication of  $YVO_4:Eu^{3+}$  nanoparticles and nanowires were achieved by microwave assisted chemical synthesis (Huong *et al.*, 2016).

Several works related the doping of  $RE^{3+}$  ions into different types of inorganic matrices (Pinatti *et al.*, 2015; 2016; 2019a; 2019b; Yang *et al.*, 2018). The RE emissions arise from the 4f–4f or 5d–4f transitions from the UV to near-IR range of electromagnetic spectrum. Also, upconverting (UC) materials are an unprecedented technology which consists of absorption of two or more lower-energy photons and subsequently emission of one higher-energy photon. This strategy is specially used for solar energy materials, bioimaging, among other applications. Materials composed of  $Yb^{3+}/Er^{3+}$  as activator ions can be efficiently excited using NIR (near-infrared) laser radiation to generate visible emission. For example, photostable and small  $YVO_4:Yb/Er$

upconversion nanoparticles in water were obtained and presented intense upconversion emission (Alkahtani *et al.*, 2021). However, many of these materials present poor luminescence efficiency and/or complicated synthesis procedure, which results in no defined or irregular sizes particles (Ji *et al.*, 2021; Kshetri *et al.*, 2018; Sousa Filho *et al.*, 2019; Woźny *et al.*, 2019).

Accordingly, in this work, we report the synthesis of  $YVO_4:RE$  (RE = Eu, Tm, and Yb/Er) nanoparticles by the microwave-assisted hydrothermal (MAH) method. These nanoparticles were structurally characterized and potentially studied in terms of its PL properties. In addition, the structure, vibrational frequency and morphology are compared to rationalize the structure, morphology, and PL emissions.

## 2. Experimental

### 2.1 Synthesis

One mmol of  $NH_4VO_3$  (99%, Sigma-Aldrich) was dissolved in 40 mL of distilled water at room temperature under magnetic stirring until the reagent was completely dissolved. Additionally, 2 mmol of  $Y(NO_3)_3 \cdot 4H_2O$  (99.999%, Sigma-Aldrich) was dissolved in 40 mL of distilled water at room temperature.  $RE(NO_3)_3$  (RE = Eu, Tm, Yb, and Er) solutions were prepared by dissolving  $RE_2O_3$  in aqueous hot solution of  $HNO_3$  and evaporating the excess of acid. Stoichiometric volume of RE solutions were mixed together with the Y solution. The amount of 5 mol% of  $Eu^{3+}$ , and  $Tm^{3+}$ ; and 5 mol%  $Yb^{3+}/2$  mol%  $Er^{3+}$  were chosen due to previous works related to maximum PL emission intensity achieved. After complete dissolution of the reactants, the V solution was mixed with the Y solution to obtain  $YVO_4$  and with the Y/RE solution to obtain  $YVO_4:RE$  nanoparticles. Subsequently, the mixture was stirred for 10 min, and, thereafter, it was transferred to the MAH system at 160 °C for 32 min, as it was the ideal conditions for many materials obtained by this methodology. The precipitates formed were collected at room temperature, washed with distilled water until the pH was neutralized, and dried in a conventional furnace at 60 °C for 12 h. Figure 1 shows a representation of the synthesis procedure herein described.

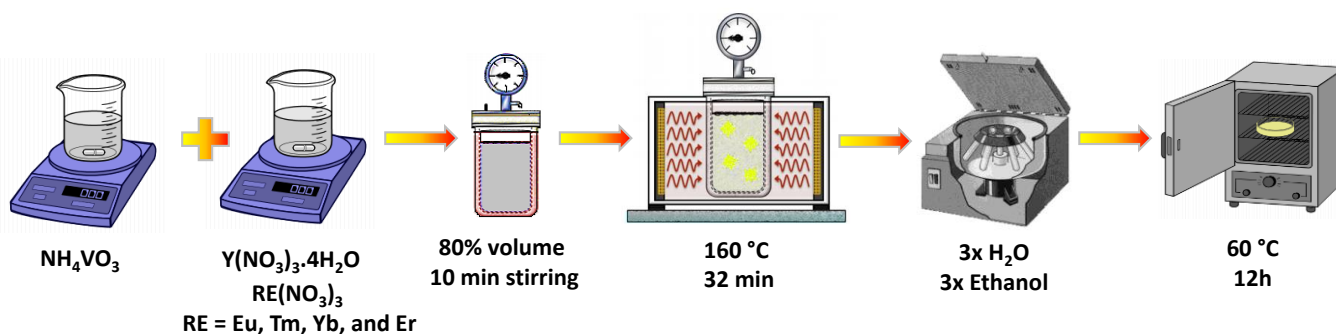


**Figure 1.** Schematic representation of synthesis procedure of the nanoparticles.

## 2.2 Characterizations

The nanoparticles were structurally characterized by X-ray diffraction (XRD) patterns using a D/Max-2000PC diffractometer Rigaku (Japan) with  $\text{Cu K}\alpha$  radiation ( $\lambda = 1.5406 \text{ \AA}$ ) in the  $2\theta$  range from  $10^\circ$  to  $80^\circ$  in the normal routine, with a scanning velocity of  $2^\circ \text{ min}^{-1}$ . This unit cell was modelled using the visualization for electronic and structural analysis (VESTA) program (Momma and Izumi, 2008; 2011), version 3. Micro-Raman spectroscopy was conducted on a Horiba Jobin-Yvon (Japan) spectrometer charge-coupled device detector and argon-ion laser (Melles Griot, United States) operating at 532 nm with a maximum power of 200 mW. The ultraviolet-visible spectrophotometry (UV-vis) spectra were taken using a spectrophotometer (model Cary 5G) (Varian, USA) in diffuse-reflectance mode. Morphological analysis of the particles was recorded via field-emission scanning electron microscopy (FE-SEM) using a Carl Zeiss microscope (model Supra 35) operated at an accelerating voltage of 30 kV and a working distance of 3.7 mm. Transmission electron microscopy (TEM) and high-resolution transmission electron microscopy (HRTEM) analysis was performed using a Jeol JEM-2100F with a field-emission gun (FEG) operating at 200 kV. For the micrographs, the samples (approximately 1 mg) were dispersed in 3 mL of distilled water and kept 15 min in the ultrasound bath. Then, one drop of the suspension was deposited on a silicon wafer, dried at room temperature and finally attached to a sample stub using carbon tape for FE-SEM analysis; and one drop of the suspension was deposited on the copper grid and dried at room temperature for TEM analysis. Photoluminescence (PL) measurements were performed by two distinct equipment. In the first one, the samples were excited by a 355 nm laser (Cobolt/Zouk) focused on a  $20 \mu\text{m}$  spot, 50  $\mu\text{W}$  of power. The backscattered luminescence was dispersed by a 20 cm spectrometer with the signal detected by a charged coupled device

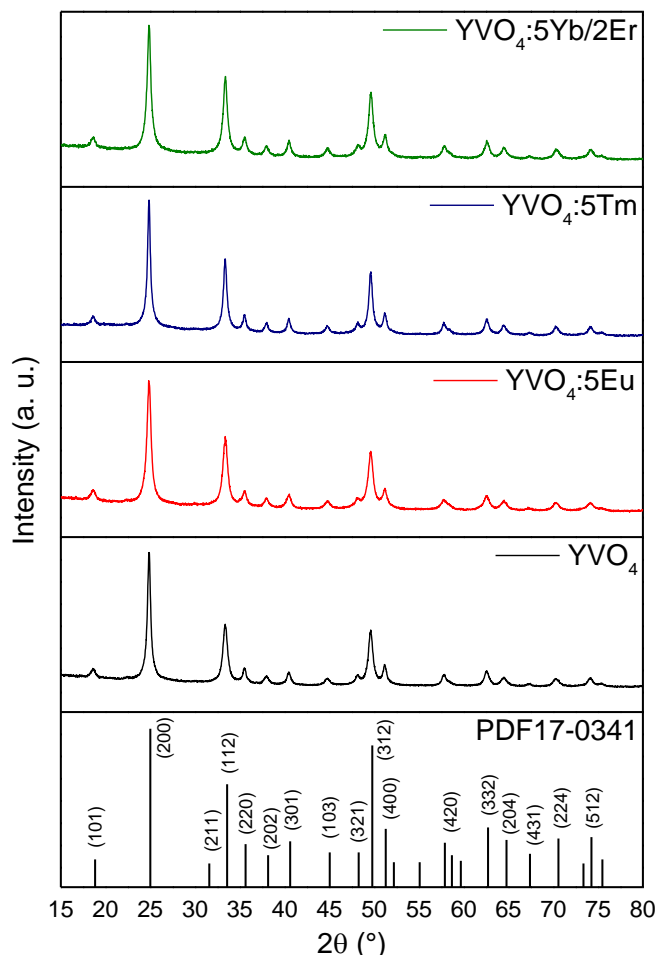
detector (Andor technologies). In the second one, the PL spectra were carried out with 325 nm excitation source of a krypton ion laser (Coherent Innova) and 200 mW laser output, at monochromator Thermal Jarrel-Ash Monospec and a Hamamatsu R446 photomultiplier. All measurements were performed at room temperature.

## 3. Results and discussion

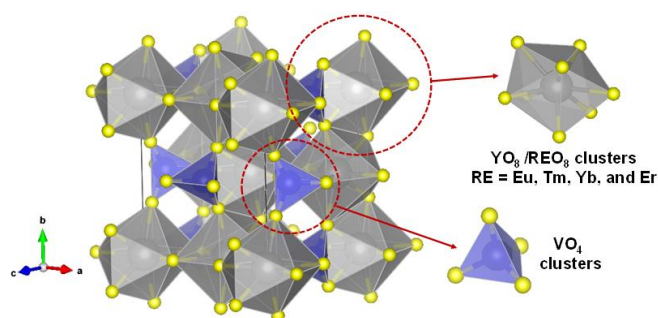
### 3.1 X-ray diffraction patterns

Figure 2 shows the XRD patterns of  $\text{YVO}_4:\text{RE}$ , and all the diffraction peaks can be readily indexed to the pure tetragonal  $\text{YVO}_4$  phase (PDF No. 17-0341) (Rivera-Enrez and Fernandez-Osorio, 2021; Yu *et al.*, 2002). The intense and sharp peaks confirm the samples are pure and present high crystallinity, as well as structural long-range order. Also,  $\text{Y}^{3+}$  site is an ideal environment with a  $\text{D}_{2d}$  point symmetry for RE emitter. So, effectively Y-by-RE substitution occurs in the host lattice because  $\text{RE}^{3+}$  and  $\text{Y}^{3+}$  have similar ionic radius, as widely reported by many works (Matos *et al.*, 2016; Rivera-Enrez and Fernandez-Osorio, 2021). This substitution was not perceived on the XRD patterns due to the limitation of detection of the XRD instrument.

A representation of the unit cell for the orthorhombic  $\text{YVO}_4:\text{RE}$  nanoparticles are presented in Fig. 3. This unit cell was modelled using the lattice parameters and atomic positions, as well as the possible RE-by-Y substitution. The Y/RE coordination environment is a distorted dodecahedral  $[\text{YO}_8]/[\text{REO}_8]$  clusters, while V is a distorted tetrahedral  $[\text{VO}_4]$  cluster.



**Figure 2.** X-ray diffraction patterns of the  $\text{YVO}_4:\text{RE}$  nanoparticles.

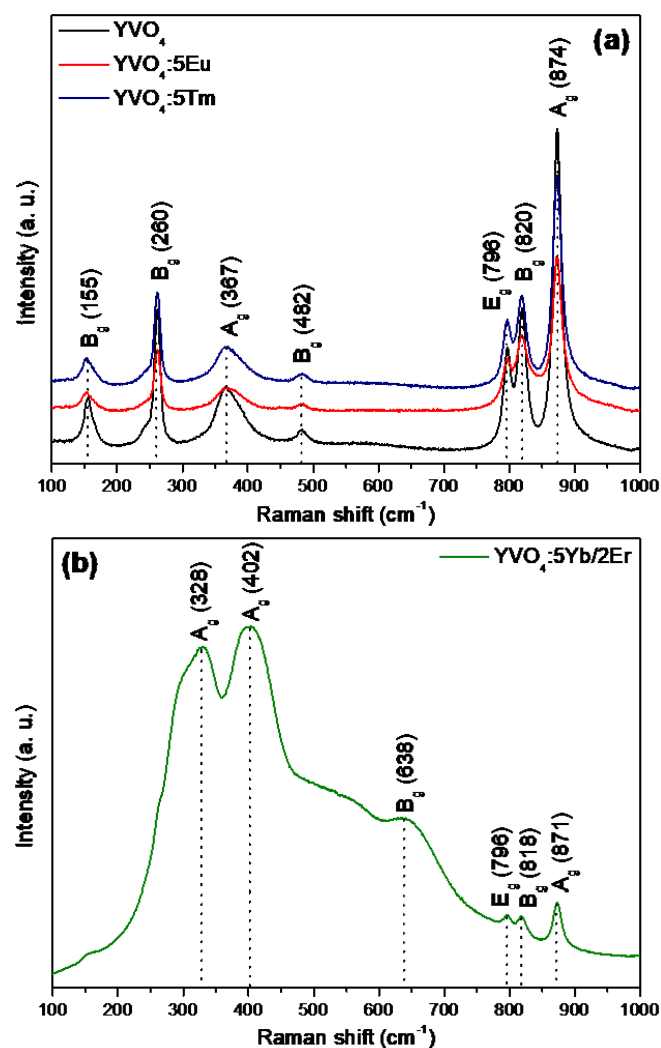


**Figure 3.** Unit cell representation of  $\text{YVO}_4:\text{RE}$  nanoparticles. Gray, blue, and yellow balls are Y/RE, V and O atoms, respectively.

### 3.2 Raman spectroscopy

Figure 4 shows the room temperature Raman spectra of  $\text{YVO}_4:\text{RE}$  nanoparticles excited by a green laser. Experimentally, seven active Raman modes were observed at 155, 260, 367, 482, 796, 820, and 874  $\text{cm}^{-1}$  for the  $\text{YVO}_4$ ,  $\text{YVO}_4:\text{5Eu}$ , and  $\text{YVO}_4:\text{5Tm}$  samples. For the  $\text{YVO}_4:\text{5Yb/2Er}$ , six active Raman modes were

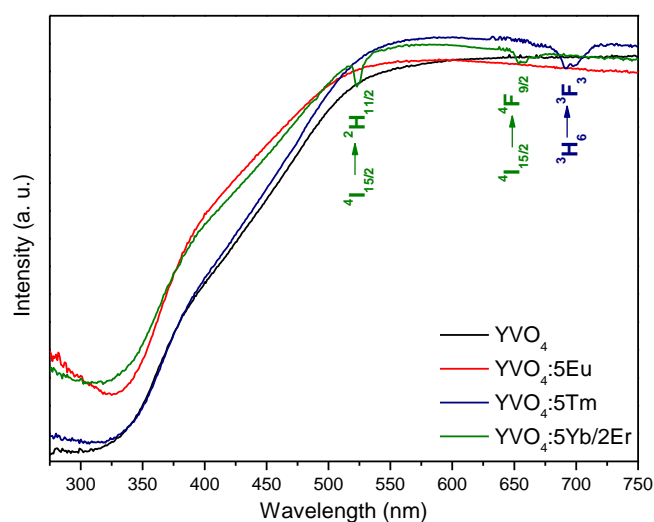
observed at 328, 402, 638, 796, 818, and 871  $\text{cm}^{-1}$ . Also, the  $\text{YVO}_4:\text{5Yb/2Er}$  nanoparticle present a broad PL emission, as observed in the Raman spectra, due to the Yb/Er ions. These results confirm the structural short-range order of all samples (Jayaraman *et al.*, 1987).



**Figure 4.** Raman spectra of the (a)  $\text{YVO}_4:\text{RE}$  (RE = Eu and Tm), and (b)  $\text{YVO}_4:\text{5Yb/2Er}$  nanoparticles.

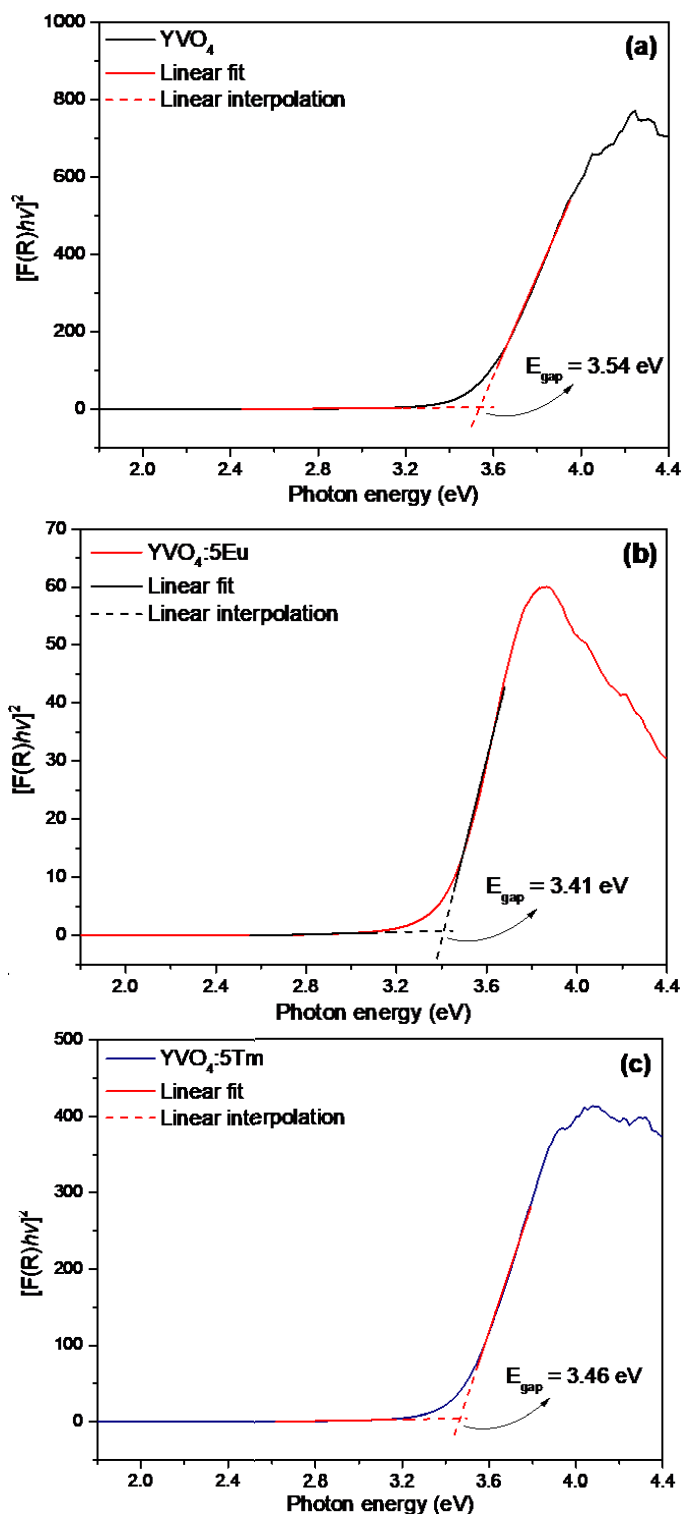
### 3.3 UV-vis spectroscopy

Figure 5 illustrates the UV-vis diffuse reflectance spectra of the  $\text{YVO}_4:\text{RE}$  nanoparticles in the range of 275–750 nm. The samples showed absorption in the ultraviolet region at approximately 450 nm. The absorption is a result of electronic transition between the valence band (VB) formed predominantly by O 2p state, and the conduction band (CB) composed mainly by V 3d states (Yang *et al.*, 2018). Also, the  $\text{YVO}_4:\text{5Tm}$  sample present the  ${}^3\text{H}_6 \rightarrow {}^3\text{F}_3$  transition, and the  $\text{YVO}_4:\text{5Yb/2Er}$  present the  ${}^4\text{I}_{15/2} \rightarrow {}^2\text{H}_J$  ( $J = 11/2$  and  $9/2$ ) transitions.



**Figure 5.** The UV-vis diffuse reflectance spectra of the  $\text{YVO}_4:\text{RE}$  nanoparticles.

The band gap energy ( $E_{\text{gap}}$ ) values were calculated using the relation of the Kubelka–Munk and Wood Tauc function, as previously reported (Pinatti *et al.*, 2019a), and it was obtained by linear extrapolation of the UV-vis curve in the  $[\text{F}(\text{R}_\infty)h\nu]^n$  versus  $h\nu$  graph.  $\text{F}(\text{R}_\infty)$  is the Kubelka–Munk function,  $h\nu$  is the photon energy, and  $n$  is a constant related to the type of electronic transition of a semiconductor ( $n = 0.5$  for direct allowed,  $n = 2$  for indirect allowed,  $n = 1.5$  for direct forbidden, and  $n = 3$  for indirect forbidden). The theoretical calculation predicts a direct allowed transition for  $\text{YVO}_4$ . Thus, the  $E_{\text{gap}}$  values obtained were 3.54, 3.41, 3.46, and 3.39 eV for the  $\text{YVO}_4$ ,  $\text{YVO}_4:5\text{Eu}$ ,  $\text{YVO}_4:5\text{Tm}$ , and  $\text{YVO}_4:5\text{Yb}/2\text{Er}$  samples, respectively (Fig. 6). These results show that the  $E_{\text{gap}}$  values decrease due to insertion of the RE ions, indicating that the degree of order-disorder at electronic level were affected due to Y-by-RE substitution. This behavior was previously observed in other RE doped materials and is attributed mainly by the contribution of  $4f^n$  electrons of  $\text{RE}^{3+}$  ions either to the VB or CB, which can increase the covalent bonding of V–O and reduce the  $E_{\text{gap}}$ . This happens because the energy level of  $\text{RE}^{3+}$  ions matches the energy level of  $\text{VO}_4^{3-}$ , contributing to an effective energy transfer from the  $\text{VO}_4^{3-}$  to the excited states of  $\text{RE}^{3+}$  ions (Yang *et al.*, 2018).



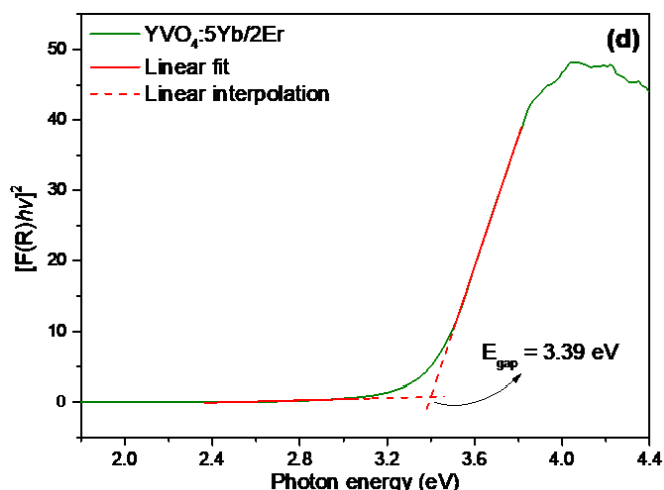


**Figure 6.** Band gap energy ( $E_{gap}$ ) for the  $YVO_4:RE$  nanoparticles.

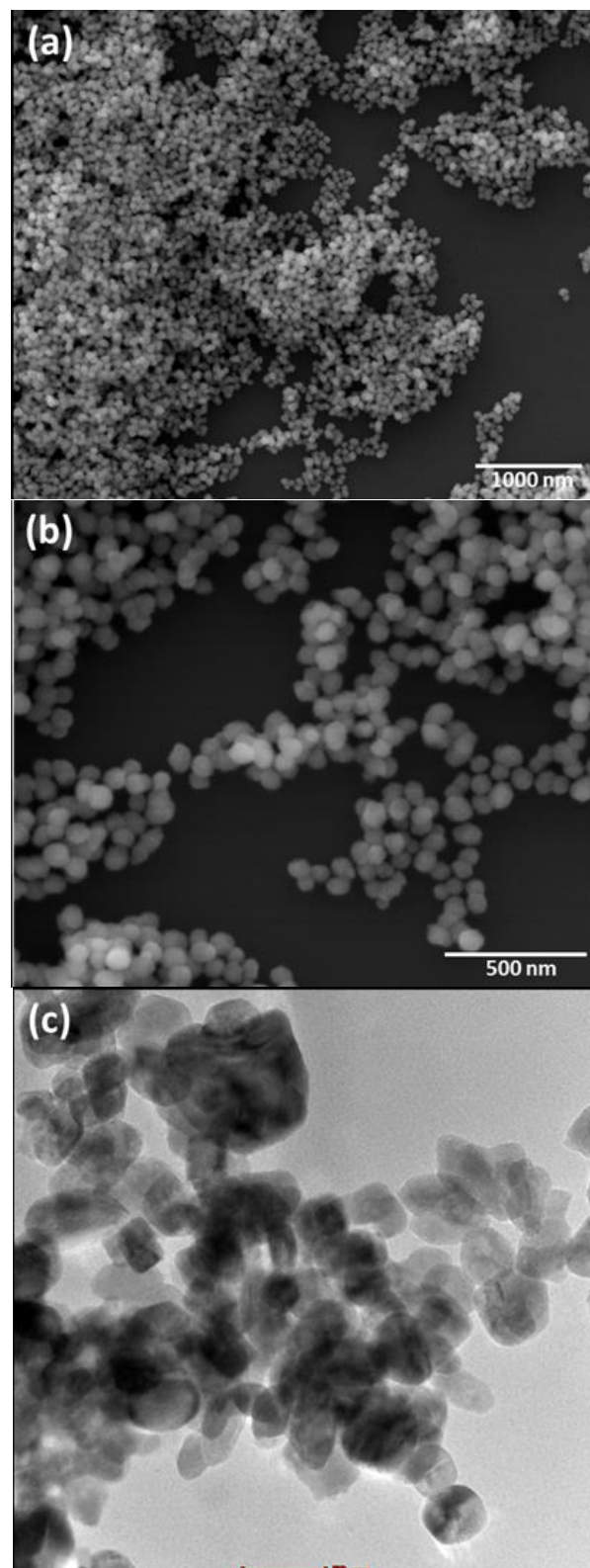
### 3.4 Field-emission scanning electron microscopy and TEM

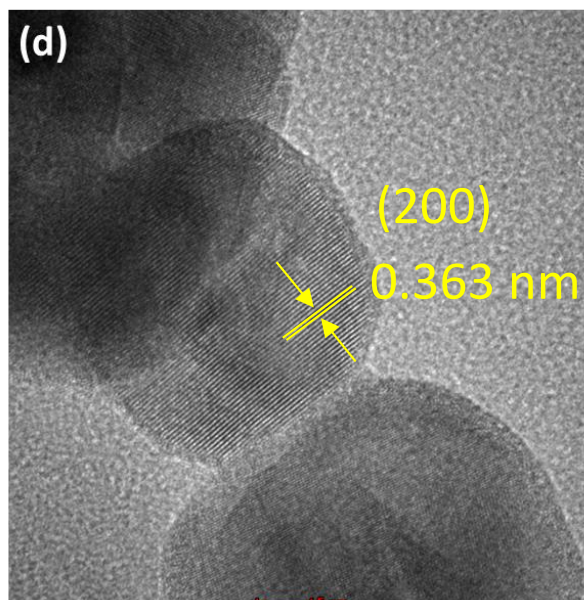
The detailed morphology and particle size of  $YVO_4$  nanoparticles were assessed by FE-SEM, and the nanostructures were further characterized by TEM and HRTEM. Field emission scanning electron microscopy micrographs of the  $YVO_4$  nanoparticles are shown in Fig. 7a and b. It is clearly seen spherical nanoparticles which exhibit a high degree of homogeneity in the shape and size. As shown in Fig. 7a and b, the particles present smooth surface, well-defined shape, and are mainly aggregated with a monodisperse size distribution.

Figure 7c shows the TEM image of  $YVO_4$  nanoparticles. It was mainly observed spherical-like particles of sizes ranging from 20 to 50 nm. Most of them have perfect circular morphology, while other present small deformations. Figure 7d shows the HRTEM image of  $YVO_4$  nanoparticles. The  $YVO_4$  nanoparticles presented a single crystalline nature and the lattice spacing was calculated to be 0.363 nm between two adjacent lattice fringes, which could be indexed to 200 planes of zircon-type  $YVO_4$ . This is in agreement with the XRD results (Shen *et al.*, 2010). Moreover, the other  $YVO_4:RE$  samples also showed similar morphology and as single-crystalline and this can be attributed to the similar preparative conditions and the low dopant concentration of  $RE^{3+}$  ions (data not shown).

These results confirm that nanosized  $YVO_4$  of spherical morphology can be obtained by the MAH method at short reactional time and low temperature. Moreover, this morphology, as well as the size, are effectively acquired without the use of surfactants, templates, organic solvents, or adjustment of pH value

of the medium, which is usually required to obtain homogeneous and nanosized particles.

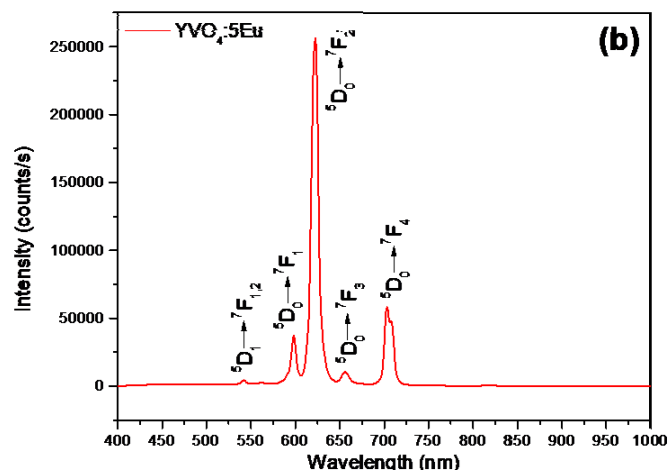
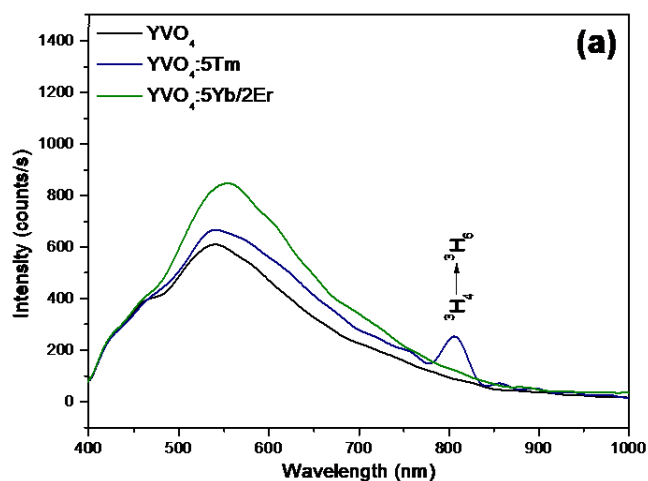




**Figure 7.** (a, b) FE-SEM images, (c) TEM image, and (d) HRTEM image of YVO<sub>4</sub> nanoparticles.

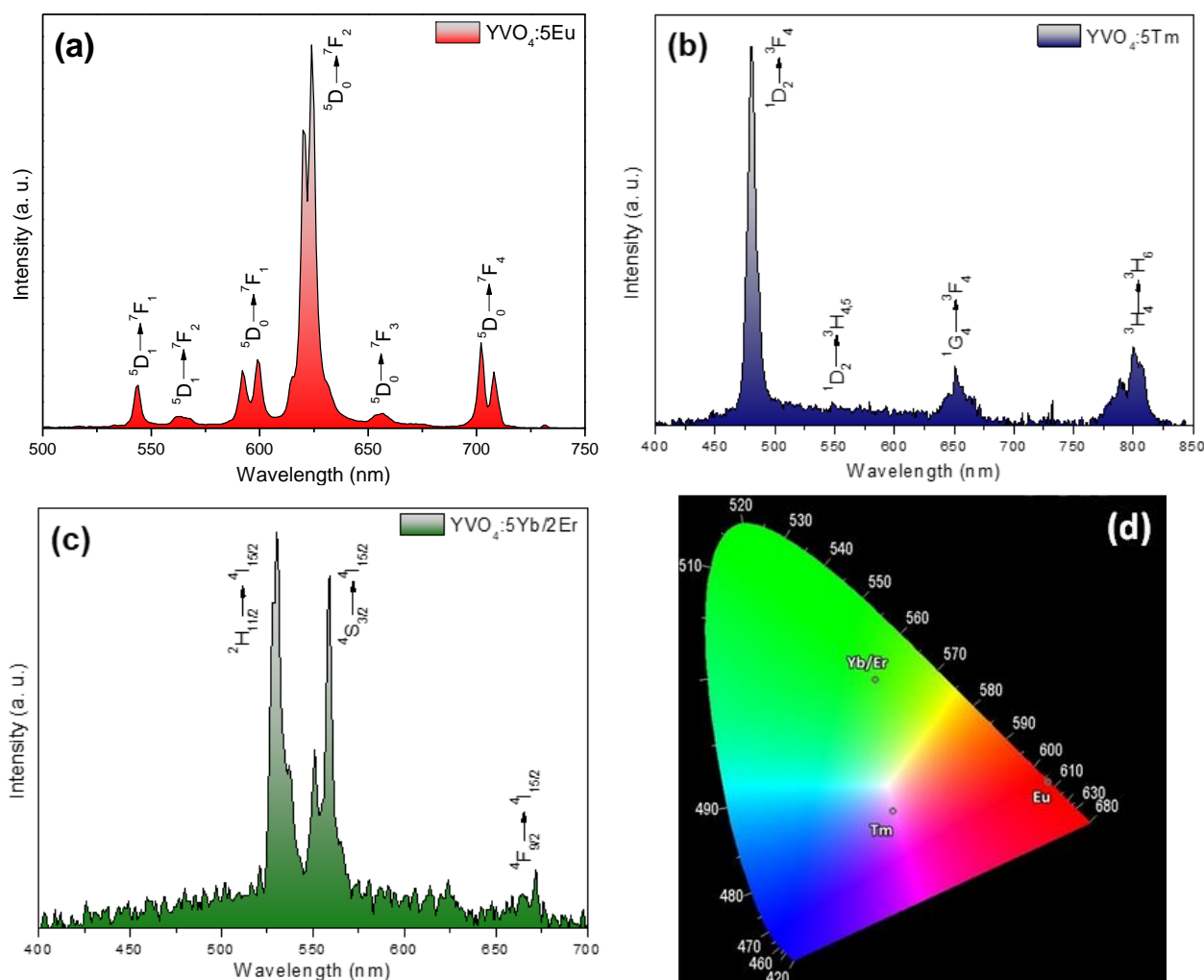
### 3.5 Photoluminescence spectroscopy

Figure 8 shows the PL emission spectra at room temperature of YVO<sub>4</sub>:RE nanoparticles under the excitation wavelength of 355 nm. Figure 8a shows the PL emission spectra of YVO<sub>4</sub>:RE (RE = Tm, and Yb/Er) nanoparticles, presenting an intense band at 540 nm due to VO<sub>4</sub><sup>3-</sup> clusters (Jin *et al.*, 2011), and the YVO<sub>4</sub>:5Tm nanoparticles also present the <sup>3</sup>H<sub>4</sub>→<sup>3</sup>H<sub>6</sub> transition at 806 nm. Particularly, the YVO<sub>4</sub>:Eu nanoparticles present intense <sup>5</sup>D<sub>1</sub>→<sup>7</sup>F<sub>J</sub> (J = 1 and 2) and <sup>5</sup>D<sub>0</sub>→<sup>7</sup>F<sub>J</sub> (J = 1–4) transitions, which arises due to the efficient energy transfer from VO<sub>4</sub><sup>3-</sup> clusters to the Eu<sup>3+</sup> ions (see Fig. 8b) (Matos *et al.*, 2016; Pinatti *et al.*, 2019a; Saltarelli *et al.*, 2014).



**Figure 8.** Photoluminescent emission spectra of (a) YVO<sub>4</sub>:RE (RE = Tm and Yb/Er), and (b) YVO<sub>4</sub>:5Eu nanoparticles.

Figure 9 shows the PL emission spectra at room temperature of YVO<sub>4</sub>:RE nanoparticles under the excitation wavelength of 325 nm, as well as the CIE chromatic diagram. Figure 9a shows the PL emission spectra of the YVO<sub>4</sub>:5Eu nanoparticles, which presents characteristic Eu<sup>3+</sup> peaks at 543, 564, 595, 622, 655, and 705 nm ascribed to the <sup>5</sup>D<sub>1</sub>→<sup>7</sup>F<sub>J</sub> (J = 1 and 2), and <sup>5</sup>D<sub>0</sub>→<sup>7</sup>F<sub>J</sub> (J = 1–4) transitions, respectively (Almeida *et al.*, 2021; Pinatti *et al.*, 2015). Figure 9b shows the PL emission spectra of the YVO<sub>4</sub>:5Tm nanoparticles, which present characteristic Tm<sup>3+</sup> peaks at 480, 548, 650, and 795 nm related to the <sup>1</sup>D<sub>2</sub>→<sup>3</sup>F<sub>J</sub> (J = 4 and 5), <sup>1</sup>G<sub>4</sub>→<sup>3</sup>F<sub>4</sub>, and <sup>3</sup>H<sub>4</sub>→<sup>3</sup>H<sub>6</sub> transitions, respectively (Pinatti *et al.*, 2019a). Figure 9c shows the PL emission spectra of the YVO<sub>4</sub>:5Yb/2Er nanoparticles, which present characteristic Er<sup>3+</sup> peaks at 530, 555, and 671 nm attributed to the <sup>2</sup>H<sub>11/2</sub>→<sup>4</sup>I<sub>15/2</sub>, <sup>4</sup>S<sub>3/2</sub>→<sup>4</sup>I<sub>15/2</sub>, and <sup>4</sup>F<sub>9/2</sub>→<sup>4</sup>I<sub>15/2</sub> transitions, respectively (Alkahtani *et al.*, 2021; Mahata *et al.*, 2015; Sun *et al.*, 2006; Woźny *et al.*, 2018; Zhang *et al.*, 2010). Figure 9d shows the CIE chromatic diagram and the respective positions of x, and y coordinates of the YVO<sub>4</sub>:RE (RE = Eu, Tm, and Yb/Er) nanoparticles obtained through the PL emission spectra. The (x,y) chromatic coordinates positions are listed in Tab. 1. The YVO<sub>4</sub>:5Eu, YVO<sub>4</sub>:5Tm, and YVO<sub>4</sub>:5Yb/2Er nanoparticles present intense emitting color in the red, blue, and green region of the diagram, respectively. These results confirm the purity and brightness of the samples and can be considered as optimum materials for optical devices.



**Figure 9.** Photoluminescent emission spectra of (a)  $\text{YVO}_4\text{:5Eu}$ , (b)  $\text{YVO}_4\text{:5Tm}$ , (c)  $\text{YVO}_4\text{:5Yb/2Er}$  nanoparticles, and (d) CIE chromatic diagram.

**Table 1.** Chromatic coordinates values obtained by the PL emission spectra of the  $\text{YVO}_4\text{:RE}$  nanoparticles.

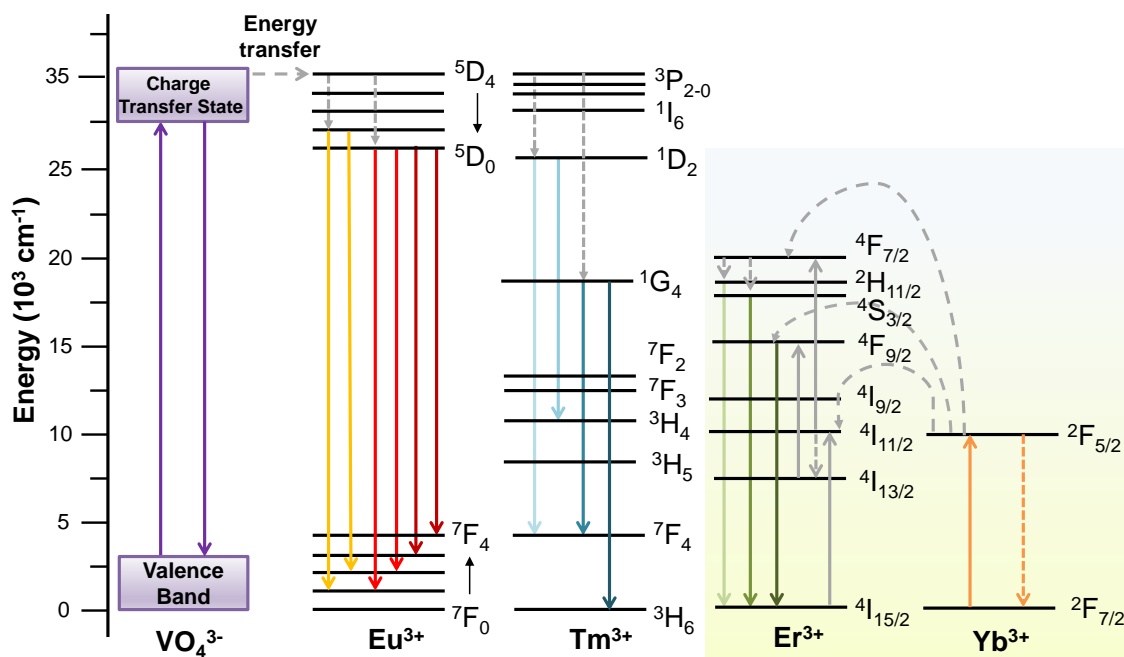
Samples	Chromatic coordinates	
	x	y
$\text{YVO}_4\text{:5Eu}$	0.65	0.34
$\text{YVO}_4\text{:5Tm}$	0.36	0.29
$\text{YVO}_4\text{:5Yb/2Er}$	0.33	0.53

Figure 10 shows a schematic energy level diagram and a proposed energy transfer mechanism for the  $\text{YVO}_4\text{:RE}$  nanoparticles. For the  $\text{YVO}_4\text{:5Eu}$  nanoparticles, it is observed that, under excitation at 325 nm, electrons are excited from VB into the charge transfer state (CTS) of the  $\text{VO}_4^{3-}$  clusters. Then, the excitation energy is transferred from the  $\text{VO}_4^{3-}$  group to the  $^5\text{D}_4$  level of  $\text{Eu}^{3+}$  cations. Afterwards,  $\text{Eu}^{3+}$  cations in the populated  $^5\text{D}_4$  level undergo multiphonon relaxation to the  $^5\text{D}_1$  level that radiatively decay to the  $^7\text{F}_j$  ( $J = 1$  and 2) levels; and to the  $^5\text{D}_0$  level that radiatively decay

to the  $^7\text{F}_j$  ( $J = 1-4$ ) levels. For the  $\text{YVO}_4\text{:5Tm}$  nanoparticles, the excitation energy is transferred from the  $\text{VO}_4^{3-}$  group to the  $^3\text{P}_2$  level of  $\text{Tm}^{3+}$  cations. Then,  $\text{Tm}^{3+}$  cations in the populated  $^3\text{P}_2$  level undergo multiphonon relaxation to the  $^1\text{D}_2$  level that radiatively decay to the  $^7\text{F}_4$  and  $^3\text{H}_4$  levels; and to the  $^1\text{G}_4$  level that radiatively decay to the  $^7\text{F}_4$  and  $^3\text{H}_6$  levels. Finally, for the  $\text{YVO}_4\text{:5Yb/2Er}$  nanoparticles, the excitation energy is transferred from the  $\text{VO}_4^{3-}$  group to the  $^4\text{F}_{7/2}$  level of  $\text{Er}^{3+}$  cations. Then,  $\text{Er}^{3+}$  cations in the populated  $^4\text{F}_{7/2}$  level undergo multiphonon relaxation to the  $^2\text{H}_{11/2}$  and  $^4\text{S}_{3/2}$  levels that radiatively decay to the  $^4\text{I}_{15/2}$  level; and to the  $^4\text{F}_{9/2}$  level that radiatively decay to the  $^4\text{I}_{15/2}$  level. Alternatively, according to the energy conservation law, a two-photon process can occur and populate the green and red UC emissions of  $\text{Er}^{3+}$  ions. The successive energy transfers are:  $^4\text{I}_{15/2}(\text{Er}^{3+}) + ^2\text{F}_{5/2}(\text{Yb}^{3+}) \rightarrow ^4\text{I}_{11/2}(\text{Er}^{3+}) + ^2\text{F}_{7/2}(\text{Yb}^{3+})$  and  $^4\text{I}_{11/2}(\text{Er}^{3+}) + ^2\text{F}_{5/2}(\text{Yb}^{3+}) \rightarrow ^4\text{F}_{7/2}(\text{Er}^{3+}) + ^2\text{F}_{7/2}(\text{Yb}^{3+})$  excite  $\text{Er}^{3+}$  ions to the  $^4\text{F}_{7/2}$  state.  $\text{Er}^{3+}$

ions at the  $^2H_{11/2}/^4S_{3/2}$  states, arising from the nonradiative relaxation (NR) process of the  $^4F_{7/2}$  state, radiatively decay to the  $^4I_{15/2}$  state, resulting the green UC emissions. The  $^4F_{9/2}$  red emitting state is populated

by the process:  $^4I_{13/2}(\text{Er}^{3+}) + ^2F_{5/2}(\text{Yb}^{3+}) \rightarrow ^4F_{9/2}(\text{Er}^{3+}) + ^2F_{7/2}(\text{Yb}^{3+})$ , where the  $^4I_{13/2}$  state is populated by NR process of the  $^4I_{11/2}$  state (Ji *et al.*, 2021).



**Figure 10.** Schematic energy level diagram and a proposed energy transfer mechanism for the YVO<sub>4</sub>:RE nanoparticles. Solid arrows = radiative transition, dashed arrows = energy transfer, and dotted arrows = nonradiative transition.

## 4. Conclusions

In summary, we reported the efficient synthesis of YVO<sub>4</sub>:RE nanoparticles by the microwave-assisted hydrothermal method. Long-range order was confirmed by XRD patterns, which showed sharp and well-defined peaks with no segregated materials. Vibrational Raman modes observed represent a signature of the structural organization in the short-range. The UV-vis spectra indicate that the band gap value decreases due to RE doping attesting structural order-disorder of the materials. The FE-SEM, TEM, and HRTEM images prove that the materials are spherical and in the nanoscale size. Photoluminescent emission spectra present transitions in the red, blue, and green regions, attesting these materials as good phosphors in the visible region. Also, the YVO<sub>4</sub>:5Yb/2Er is a good candidate as promising material for UC phosphor.

## Authors' contribution

**Conceptualization:** Pinatti, I. M.; Foggi, C. C.; Teodoro, M. D.; Longo, E.; Simões, A. Z.; Rosa, I. L. V.

**Data curation:** Pinatti, I. M.; Foggi, C. C.; Teodoro, M. D.; Longo, E.; Simões, A. Z.; Rosa, I. L. V.

**Formal Analysis:** Pinatti, I. M.; Foggi, C. C.; Teodoro, M. D.; Longo, E.; Simões, A. Z.; Rosa, I. L. V.

**Funding acquisition:** Pinatti, I. M.; Foggi, C. C.; Teodoro, M. D.; Longo, E.; Simões, A. Z.; Rosa, I. L. V.

**Investigation:** Pinatti, I. M.; Foggi, C. C.; Teodoro, M. D.; Longo, E.; Simões, A. Z.; Rosa, I. L. V.

**Methodology:** Pinatti, I. M.; Foggi, C. C.; Teodoro, M. D.; Longo, E.; Simões, A. Z.; Rosa, I. L. V.

**Project administration:** Pinatti, I. M.; Foggi, C. C.; Teodoro, M. D.; Longo, E.; Simões, A. Z.; Rosa, I. L. V.

**Resources:** Pinatti, I. M.; Foggi, C. C.; Teodoro, M. D.; Longo, E.; Simões, A. Z.; Rosa, I. L. V.

**Software:** Not applicable.

**Supervision:** Longo, E.; Simões, A. Z.; Rosa, I. L. V.

**Validation:** Pinatti, I. M.; Foggi, C. C.; Teodoro, M. D.; Longo, E.; Simões, A. Z.; Rosa, I. L. V.

**Visualization:** Pinatti, I. M.; Foggi, C. C.; Teodoro, M. D.; Longo, E.; Simões, A. Z.; Rosa, I. L. V.

**Writing – original draft:** Pinatti, I. M.; Foggi, C. C.; Teodoro, M. D.; Longo, E.; Simões, A. Z.; Rosa, I. L. V.

**Writing – review & editing:** Pinatti, I. M.; Foggi, C. C.; Teodoro, M. D.; Longo, E.; Simões, A. Z.; Rosa, I. L. V.

## Data availability statement

The data will be available upon request.

## Funding

Fundação de Amparo à Pesquisa do Estado de São Paulo (FAPESP). Grant No.: 13/07296-2; 17/12594-3; 19/03722-3; 19/25944-8.

## Acknowledgments

The authors would like to acknowledge Maximo Siu Li (IFSC-USP), Rorivaldo Camargo (CDMF-UFSCar), and Sandra Maria Terenzi Bellini (CDMF-UFSCar) for technical and scientific contributions.

This manuscript is dedicated to the memory of Professor Dr. José Arana Varela, pioneer with notable achievements in the fields of materials science, physics and chemistry. He was one of the founders of the Interdisciplinary Laboratory of Electrochemistry and Ceramics (LIEC), Brazil. Dr. Varela contributed significantly to the development of Brazilian science, and had an outstanding international reputation as an educator and researcher.

## References

- Alkahtani, M.; Alfahd, A.; Alsofyani, N.; Almuqhim, A. A.; Qassem, H.; Alshehri, A. A.; Almughen, F. A.; Hemmer, P. Photostable and small YVO<sub>4</sub>:Yb,Er upconversion nanoparticles in water. *Nanomaterials* **2021**, *11* (6), 1535. <https://doi.org/10.3390/nano11061535>
- Almeida, P. B.; Pinatti, I. M.; Oliveira, R. C.; Teixeira, M. M.; Santos, C. C.; Machado, T. R.; Longo, E.; Rosa, I. L. V. Structural, morphological and photoluminescence properties of β-Ag<sub>2</sub>MoO<sub>4</sub> doped with Eu<sup>3+</sup>. *Chem. Pap.* **2021**, *75*, 1869–1882. <https://doi.org/10.1007/s11696-020-01489-4>
- Ferreira, N. H.; Furtado, R. A.; Ribeiro, A. B.; Oliveira, P. F.; Ozelin, S. D.; Souza, L. D. R.; Rinaldi Neto, F.; Miura, B. A.; Magalhães, G. M.; Nassar, E. J.; Tavares, D. C. Europium(III)-doped yttrium vanadate nanoparticles reduce the toxicity of cisplatin. *J. Inorg. Biochem.* **2018**, *182*, 9–17. <https://doi.org/10.1016/j.jinorgbio.2018.01.014>
- Huong, T. T.; Vinh, L. T.; Phuong, H. T.; Khuyen, H. T.; Anh, T. K.; Tu, V. D.; Minh, L. Q. Controlled fabrication of the strong emission YVO<sub>4</sub>:Eu<sup>3+</sup> nanoparticles and nanowires by microwave assisted chemical synthesis. *J. Lumin.* **2016**, *173*, 89–93. <https://doi.org/10.1016/j.jlumin.2016.01.003>
- Jayaraman, A.; Kourouklis, G. A.; Espinosa, G. P.; Cooper, A. S.; Van Uitert, L. G. A high-pressure Raman study of yttrium vanadate (YVO<sub>4</sub>) and the pressure-induced transition from the zircon-type to the scheelite-type structure. *J. Phys. Chem. Solids* **1987**, *48* (8), 755–759. [https://doi.org/10.1016/0022-3697\(87\)90072-2](https://doi.org/10.1016/0022-3697(87)90072-2)
- Ji, H.; Tang, J.; Tang, X.; Yang, Z.; Zhang, H.; Qian, Y. Enhanced upconversion emissions of NaNbO<sub>3</sub>:Er<sup>3+</sup>/Yb<sup>3+</sup> nanocrystals via Mg<sup>2+</sup> ions doping. *Mater. Lett.* **2021**, *302*, 130348. <https://doi.org/10.1016/j.matlet.2021.130348>
- Jin, Y.; Li, C.; Xu, Z.; Cheng, Z.; Wang, W.; Li, G.; Lin, J. Microwave-assisted hydrothermal synthesis and multicolor tuning luminescence of YP<sub>x</sub>V<sub>1-x</sub>O<sub>4</sub>:Ln<sup>3+</sup> (Ln = Eu, Dy, Sm) nanoparticles. *Mater. Chem. Phys.* **2011**, *129* (1–2), 418–423. <https://doi.org/10.1016/j.matchemphys.2011.04.035>
- Kshetri, Y. K.; Regmi, C.; Kim, H.-S.; Lee, S. W.; Kim, T. H. Microwave hydrothermal synthesis and upconversion properties of Yb<sup>3+</sup>/Er<sup>3+</sup> doped YVO<sub>4</sub> nanoparticles. *Nanotechnology* **2018**, *29* (20), 204004. <https://doi.org/10.1088/1361-6528/aab2bf>
- Li, K.; Chen, T.; Mao, H.; Chen, Y.; Wang, J. Preparation and Upconversion Emission Investigation of the YVO<sub>4</sub>:Yb<sup>3+</sup>:Er<sup>3+</sup> Nanomaterials and Their Coupling with the Au Nanoparticles. *J. Electron. Mater.* **2021**, *50*, 1189–1195. <https://doi.org/10.1007/s11664-020-08636-3>
- Liu, Y.; Xiong, H.; Zhang, N.; Leng, Z.; Li, R.; Gan, S. Microwave synthesis and luminescent properties of YVO<sub>4</sub>:Ln<sup>3+</sup> (Ln = Eu, Dy and Sm) phosphors with different morphologies. *J. Alloys Compd.* **2015**, *653*, 126–134. <https://doi.org/10.1016/j.jallcom.2015.09.015>
- Liu, Y.; Yang, C.; Xiong, H.; Zhang, N.; Leng, Z.; Li, R.; Gan, S. Surfactant assisted synthesis of the YVO<sub>4</sub>:Ln<sup>3+</sup> (Ln = Eu, Dy, Sm) phosphors and shape-dependent luminescence properties. *Colloids Surf. A Physicochem. Eng. Asp.* **2016**, *502*, 139–146. <https://doi.org/10.1016/j.colsurfa.2016.05.006>
- Mahata, M. K.; Kumar, K.; Rai, V. K. Er<sup>3+</sup>–Yb<sup>3+</sup> doped vanadate nanocrystals: A highly sensitive thermographic phosphor and its optical nanoheater behavior. *Sens. Actuators B Chem.* **2015**, *209*, 775–780. <https://doi.org/10.1016/j.snb.2014.12.039>
- Matos, M. G.; Rocha, L. A.; Nassar, E. J.; Verelst, M. Influence of Bi<sup>3+</sup> ions on the excitation wavelength of the YVO<sub>4</sub>:Eu<sup>3+</sup> matrix. *Opt. Mater.* **2016**, *62*, 12–18. <https://doi.org/10.1016/j.optmat.2016.09.035>

- Momma, K.; Izumi, F. VESTA: a three-dimensional visualization system for electronic and structural analysis. *J. Appl. Cryst.* **2008**, *41*, 653–658. <https://doi.org/10.1107/S0021889808012016>
- Momma, K.; Izumi, F. VESTA 3 for three-dimensional visualization of crystal, volumetric and morphology data. *J. Appl. Cryst.* **2011**, *44*, 1272–1276. <https://doi.org/10.1107/S0021889811038970>
- Panayiotakis, G.; Cavouras, D.; Kandarakis, I.; Nomicos, C. A study of X-ray luminescence and spectral compatibility of europium-activated yttrium-vanadate (YVO<sub>4</sub>:Eu) screens for medical imaging applications. *Appl. Phys. A* **1996**, *62*, 483–486. <https://doi.org/10.1007/BF01567121>
- Pinatti, I. M.; Nogueira, I. C.; Pereira, W. S.; Pereira, P. F. S.; Gonçalves, R. F.; Varela, J. A.; Longo, E.; Rosa, I. L. V. Structural and photoluminescence properties of Eu<sup>3+</sup> doped  $\alpha$ -Ag<sub>2</sub>WO<sub>4</sub> synthesized by the green coprecipitation methodology. *Dalton Trans.* **2015**, *44* (40), 17673–17685. <https://doi.org/10.1039/C5DT01997D>
- Pinatti, I. M.; Mazzo, T. M.; Gonçalves, R. F.; Varela, J. A.; Longo, E.; Rosa, I. L. V. CaTiO<sub>3</sub> and Ca<sub>1-3x</sub>Sm<sub>x</sub>TiO<sub>3</sub>: Photoluminescence and morphology as a result of Hydrothermal Microwave Methodology. *Ceram. Int.* **2016**, *42* (1) (Part B), 1352–1360. <https://doi.org/10.1016/j.ceramint.2015.09.074>
- Pinatti, I. M.; Fern, G. R.; Longo, E.; Ireland, T. G.; Pereira, P. F. S.; Rosa, I. L. V.; Silver, J. Luminescence properties of  $\alpha$ -Ag<sub>2</sub>WO<sub>4</sub> nanorods co-doped with Li<sup>+</sup> and Eu<sup>3+</sup> cations and their effects on its structure. *J. Lumin.* **2019a**, *206*, 442–454. <https://doi.org/10.1016/j.jlumin.2018.10.104>
- Pinatti, I. M.; Pereira, P. F. S.; Assis, M.; Longo, E.; Rosa, I. L. V. Rare earth doped silver tungstate for photoluminescent applications. *J. Alloys Compd.* **2019b**, *771*, 433–447. <https://doi.org/10.1016/j.jallcom.2018.08.302>
- Rivera-Enríquez, C. E.; Fernández-Osorio, A. L. Synthesis of YVO<sub>4</sub>:Eu<sup>3+</sup> nanophosphors by the chemical coprecipitation method at room temperature. *J. Lumin.* **2021**, *236*, 118110. <https://doi.org/10.1016/j.jlumin.2021.118110>
- Saltarelli, M.; Matos, M. G.; Faria, E. H.; Ciuffi, K. J.; Rocha, L. A.; Nassar, E. J. Preparation of YVO<sub>4</sub>:Eu<sup>3+</sup> at low temperature by the hydrolytic sol-gel methodology. *J. Sol-Gel Sci. Technol.* **2014**, *73*, 283–292. <https://doi.org/10.1007/s10971-014-3525-z>
- Shen, J.; Sun, L. D.; Zhu, J. D.; Wei, L. H.; Sun, H. F.; Yan, C. H. Biocompatible bright YVO<sub>4</sub>:Eu nanoparticles as versatile optical bioprobes. *Adv. Funct. Mater.* **2010**, *20* (21), 3708–3714. <https://doi.org/10.1002/adfm.201001264>
- Sousa Filho, P. C.; Alain, J.; Leménager, G.; Larquet, E.; Fick, J.; Serra, O. A.; Gacoin, T. Colloidal Rare Earth Vanadate Single Crystalline Particles as Ratiometric Luminescent Thermometers. *J. Phys. Chem. C* **2019**, *123* (4), 2441–2450. <https://doi.org/10.1021/acs.jpcc.8b12251>
- Sun, Y.; Liu, H.; Wang, X.; Kong, X.; Zhang, H. Optical spectroscopy and visible upconversion studies of YVO<sub>4</sub>:Er<sup>3+</sup> nanocrystals synthesized by a hydrothermal process. *Chem. Mater.* **2006**, *18*, 2726–2732. <https://doi.org/10.1021/cm051971m>
- Woźny, P.; Szczeszak, A.; Lis, S. Effect of various surfactants on changes in the emission color chromaticity in upconversion YVO<sub>4</sub>: Yb<sup>3+</sup>, Er<sup>3+</sup> nanoparticles. *Opt. Mater.* **2018**, *76*, 400–406. <https://doi.org/10.1016/j.optmat.2018.01.009>
- Woźny, P.; Runowski, M.; Lis, S. Emission color tuning and phase transition determination based on high-pressure up-conversion luminescence in YVO<sub>4</sub>: Yb<sup>3+</sup>, Er<sup>3+</sup> nanoparticles. *J. Lumin.* **2019**, *209*, 321–327. <https://doi.org/10.1016/j.jlumin.2019.02.008>
- Yang, L.; Peng, S.; Zhao, M.; Yu, L. New synthetic strategies for luminescent YVO<sub>4</sub>:Ln<sup>3+</sup> (Ln = Pr, Sm, Eu, Tb, Dy, Ho, Er) with mesoporous cell-like nanostructure. *Opt. Mater. Express* **2018**, *8*, 3805–3819. <https://doi.org/10.1364/OME.8.003805>
- Yu, M.; Lin, J.; Wang, Z.; Fu, J.; Wang, S.; Zhang, H. J.; Han, Y. C. Fabrication, patterning, and optical properties of nanocrystalline YVO<sub>4</sub>:A (A = Eu<sup>3+</sup>, Dy<sup>3+</sup>, Sm<sup>3+</sup>, Er<sup>3+</sup>) phosphor films via sol-gel soft lithography. *Chem. Mater.* **2002**, *14*, 2224–2231. <https://doi.org/10.1021/cm011663y>
- Zhang, Y.-m.; Li, Y.-h.; Li, P.; Hong, G.-y.; Yu, Y.n. Preparation and upconversion luminescence of YVO<sub>4</sub>:Er<sup>3+</sup>, Yb<sup>3+</sup>. *Int. J. Miner. Metall. Mater.* **2010**, *17*, 225–228. <https://doi.org/10.1007/s12613-010-0218-7>